# Stator-Rotor Differential Protection for Wound-Rotor Generators

Bogdan Kasztenny, Dale Finney, and Douglas Taylor
*Schweitzer Engineering Laboratories, Inc.*

Presented at the
79th Annual Georgia Tech Protective Relaying Conference
Atlanta, Georgia
April 15–17, 2026

Previously presented at the
79th Annual Conference for Protective Relay Engineers, March 2026

Originally presented at the
52nd Annual Western Protective Relay Conference, October 2025

# Stator-Rotor Differential Protection for Wound-Rotor Generators

Bogdan Kasztenny, Dale Finney, and Douglas Taylor
*Schweitzer Engineering Laboratories, Inc.*

***Abstract*—This paper focuses on rotor protection for wound-rotor asynchronous generators, often referred to as doubly fed induction generators. This paper introduces and explains a new kind of differential protection element that balances ampere-turns between the stator winding and the rotating rotor winding. Because the differential element monitors ampere-turns, it is capable of detecting both turn and phase faults in both of the windings. The presented differential element uses only currents and requires neither the stator and rotor voltages nor an encoder for the rotor position. The differential element is instantaneous and can operate on the order of one to two power cycles.**

## I. Introduction

Protection engineers have been working on addressing protection issues related to doubly fed induction generators (DFIGs) for several decades now. These generators allow a wide range of rotor speeds, making them well-suited for use in wind turbine generation (WTG) applications. Over the years, these machines have grown in size from a 1 MW range to several megawatts. The focus so far has been on protecting the network in the vicinity of DFIGs. The DFIG itself is typically protected by the manufacturer with only basic protection applied at the stator side and proprietary protection built into the converter on the rotor side [1]. This minimalistic approach is partially justified by the small power rating of DFIGs in WTG applications and the economic pressures on the WTG projects.

Recently, DFIG technology has been used or proposed for new applications where adjustable speed is beneficial. These applications include pumped storage hydro (PSH) generation and synchronous condenser (SC) installations. In these applications, the machines are rated at tens or hundreds of megawatts. We refer to these machines as wound-rotor asynchronous generators (WRAG), a name that is technically more correct than DFIG. DFIGs force the rotor currents by using converters rather than allow the currents to be induced by the rotor slip.

Section II discusses the benefits of using large-sized wound-rotor asynchronous generators in pumped storage hydro and synchronous condenser applications. We are not advocating for replacing synchronous generators with power-electronic-controlled wound-rotor asynchronous generators, but we recognize that if substantial operational benefits can be obtained at little or no additional cost, the industry is likely to adopt the new technology even if it causes new problems for network and generator protection. The short-circuit current contribution of such large-scale wound-rotor asynchronous generators and the network protection considerations are outside the scope of this paper.

Instead, this paper focuses on protecting the generator itself. Section III summarizes the requirements and challenges when protecting wound-rotor asynchronous generators, including turn faults in the stator and rotor.

Section IV introduces a new type of differential protection element that spans both the stator and rotor. Based on the ampere-turn balance between the stator and rotor, the new protection element detects phase and turn faults in either of the windings. The element does not need voltages to obtain the rotating reference frames for the stator and rotor. Neither does it need the rotor position encoder to further align the stator and rotor reference frames. Section IV discusses several application considerations, such as current measurement, current polarity, current transformer (CT) saturation during external faults, and obtaining the turn-ratio setting.

Section V describes test results based on a scaled-down 220 V, 10 hp physical model of a wound-rotor asynchronous machine. We use the physical model to validate and illustrate the new protection element. This section is primarily focused on protection security because of our limited ability to place internal faults in the physical model.

Section VI describes test results based on a digital model of a 333 MW wound-rotor asynchronous machine. Taking advantage of the digital model, we simulated a wide range of scenarios, including internal faults.

Section VII summarizes the paper and our findings.

## II. Drivers for Large Wound-Rotor Asynchronous Generators

The development of adjustable-speed machines in WTG applications has played an important role in the growth of wind energy over the last two decades. The technology used by an adjustable-speed PSH unit is essentially the same as that used by a WTG unit. PSH units, however, have much larger MVA ratings than the WTG units that are based on the DFIGs, and the PSH units involve both the turbine (generating) and pumping (motoring) modes of operation. The advantages of adjustable-speed PSH units are described in [2] and briefly summarized below.

### *A. Adjustable-Speed PSH Unit Applications*

The adjustable-speed PSH units share some similarities with conventional PSH units. For example, in order to transition from generating to pumping, the adjustable-speed PSH unit

needs to disconnect from the grid and come to a complete stop. A reversing switch at the stator terminals is then used to transpose two phases to change the rotation direction.

Also, both conventional and adjustable-speed PSH units need a starting method when in the pumping mode. A variety of methods have been used to start conventional PSH units. A converter link operated as an adjustable-speed drive (ASD) is often used. The adjustable-speed PSH unit trades this converter link for a larger converter link that feeds the rotor of the wound-rotor asynchronous machine, as shown in Fig. 1.

The stator-side and rotor-side converters in Fig. 1 have individual controllers. Typically, these controllers use the d-axis and q-axis of Park's transform currents to decouple the regulation of real and reactive power [3]. The details of converter controls are out of scope for this paper except to say that rotor speed, dc link voltage, as well as real and imaginary components of the rotor currents are all controllable via the converter control loops.

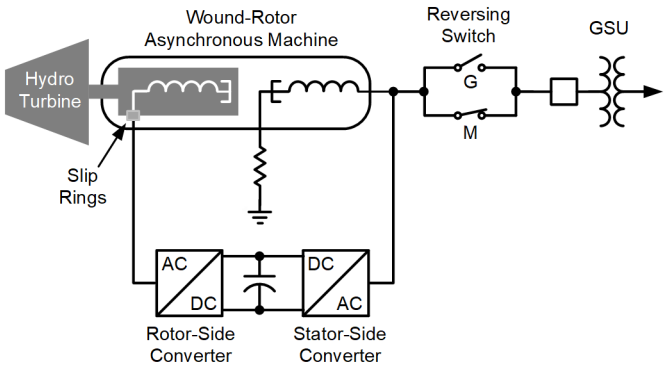


Fig. 1. Adjustable-speed PSH unit application using a wound-rotor asynchronous machine.

Adjustable-speed PSH unit applications with wound-rotor asynchronous machines provide the following benefits over PSH unit applications that use traditional synchronous machines.

*1) Increased Efficiency*

In the PSH unit generating mode for a given rotor speed, there is a specific flow of water through the turbine that results in the most efficient transfer of power to the generator. Fig. 2 plots the contours of constant turbine efficiency on a per-unit speed and per-unit flow plane. These lines define a turbine "efficiency hill". For maximum efficiency in fixed-speed PSH units, the turbine must be operated at the speed corresponding to the peak of the hill (vertical dashed line shown in Fig. 2). The same is true in the PSH unit pumping mode.

Adjustable-speed PSH units maximize efficiency by using an optimal speed for a given flow (power set point and reservoir water level) in both generating and pumping modes [4]. A variable-speed PSH unit follows the ridge of the efficiency hill (blue solid line shown in Fig. 2) by changing the speed when the flow changes.

Storage systems, including PSH systems, are evaluated according to their round-trip efficiency, which is the product of the achieved efficiencies during generating and pumping. The adjustable-speed PSH units benefit even more from the round-trip efficiency. For example, if the generating and pumping efficiencies are each 0.8 pu, the round-trip efficiency is 0.64 pu. Improving the efficiency by 0.1 pu in both the generating and pumping modes results in the round-trip efficiency of 0.81 pu – a gain of 0.17 pu.

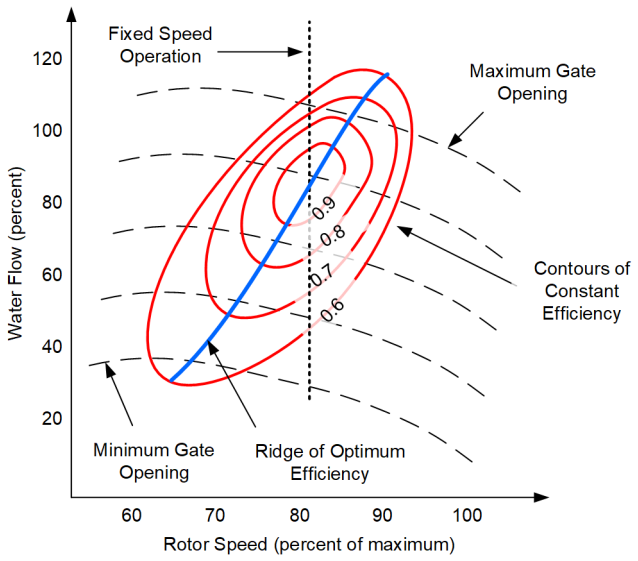


Fig. 2. Turbine efficiency plot example.

*2) Improved Dynamic Response*

The wound-rotor asynchronous generator torque ($T_E$) is a function of the product of the stator and rotor currents [5]:

$$T_E = \frac{3}{4} \cdot P \cdot L_M \cdot \left(i_{Sq} \cdot i_{Rd} - i_{Sd} \cdot i_{Rq}\right) \quad (1)$$

where:

$i_{Sd}$ and $i_{Sq}$ are stator d-axis and q-axis currents.
$i_{Rd}$ and $i_{Rq}$ are rotor d-axis and q-axis currents referred to the stator by using the turns ratio.
$P$ is the number of poles.
$L_M$ is the magnetizing inductance.

The controllers of the rotor-side converter regulate the rotor d-axis and q-axis current components almost instantaneously. Therefore, based on (1), we can control the electric torque and the output power almost instantaneously to match a sudden load change. The rotor slows down or speeds up following the load change and rotor-side control action, at which point the governor re-establishes the desired speed by adjusting the gates [4]. The fast response of the converter controls allows the governor response to be relaxed. The result is much better frequency regulation. Effectively, the rotor current frequency acts as an elastic buffer between the system frequency and the rotor speed during dynamic changes in the load.

*3) Reduced Turbine Blade Wear*

Blade cavitation and draft tube pulsations can occur when a conventional PSH unit operates at the high or low end of its output power range [6]. Therefore, the high and low operating regions are avoided to limit turbine wear. Adjustable-speed PSH unit operation allows for the speed to be varied with load, which provides improved operation over a wider range of speeds. Again, the rotor current frequency acts as an elastic buffer between the system frequency and the mechanical speed,

allowing the speed to remain within the desired turbine wear limits regardless of the output power.

In addition, conventional PSH units rely completely on gate control to regulate speed and real power. As already mentioned, the wound-rotor asynchronous generator provides a second control method, via the regulation of the rotor currents, which is faster and nonmechanical. As a result, the gates in the adjustable-speed units are not required to move as quickly or as frequently as those in conventional PSH units, reducing the duty on the gates and their actuators.

Of course, in PSH installations composed of several small units, the above benefits are less significant because individual units can be dispatched as the load changes. However, in PSH installations comprising large units, the listed benefits are quite compelling, potentially driving adoption of the adjustable-speed PSH units.

### *B. Synchronous Condensers*

Historically, SCs have been used to provide reactive power for voltage support. Rotor inertia also helps to improve transient stability. Recently, to alleviate the impact of inverter-based resources (IBRs) on system inertia and fault currents, SCs have been deployed to improve transient stability and increase fault current to aid correct protection operation. In these applications, SC inertia may be further increased with the addition of a flywheel.

Asynchronous condensers have been proposed in the literature [7] [8] [9]. These applications use a wound-rotor asynchronous generator rather than a synchronous generator. We are not aware of any asynchronous condensers installed in actual power systems.

In addition to the provision of reactive power, adjustable-speed operation allows the condenser to exchange real power between the power system and the rotating mass while operating within the rotor (and flywheel, if installed) speed limits. Consequently, although the asynchronous condenser cannot regulate frequency, it can improve transient stability in low-inertia power systems.

It is worth pointing out that the converters reduce the wound-rotor asynchronous generator fault-current contribution during system faults and make the fault current different than that of a synchronous generator. As a result, asynchronous condensers are not a solution to the IBR-reduced fault-current contribution problem.

## III. General Protection Considerations for Large Wound-Rotor Asynchronous Generators

Wound-rotor asynchronous generators can be rated at upwards of several hundred megawatts. Therefore, fast, secure, and dependable protection of these generators is critical. Until recently, research into protection methods for machines of this type has been sparce. This lack of research can be attributed to the relatively recent appearance of these generators in the power system, their small size, and the cost pressures on WTG projects.

### *A. Overview*

Protection of synchronous generators is a well-established field. Because of the similarities between synchronous generators and wound-rotor asynchronous generators, we can protect the latter by applying or adapting many synchronous generator protection schemes, such as the one shown in Fig. 3.

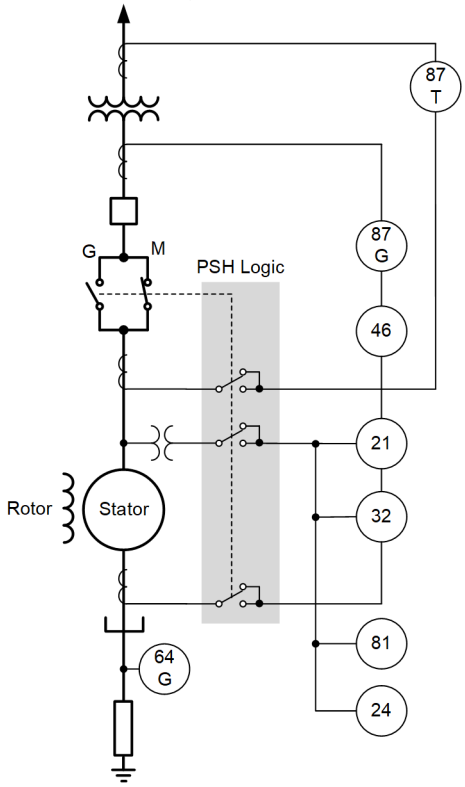


Fig. 3. Adjustable-speed PSH unit one-line protection diagram (rotor protection not shown).

The stator differential protection element and the stator ground fault protection element provide protection for phase and ground faults on the stator. In addition, conventional protection functions detect motoring, overexcitation, system faults, abnormal frequency, and unbalanced currents.

### *B. Rotor Protection Challenges*

Because the rotor circuit is supplied via brushes and slip rings, only one end of the rotor winding is accessible for rotor current measurement. This lack of access to currents on both ends of the rotor prevents the application of a conventional differential protection element based on Kirchhoff's current law.

The rotor speed in wound-rotor asynchronous generators is expected to be at or near synchronous speed for extended periods, resulting in rotor currents being dc currents or of very low frequency. Rotor current measurement is therefore another challenge.

### *C. Turn Faults*

Turn faults in generators are difficult to detect because they do not upset the current balance in a differential protection element that is based on Kirchhoff's current law. In [10], we proposed a method for detecting stator and rotor turn faults in

synchronous generators. In the following section, we propose a similar method for wound-rotor asynchronous generators.

## IV. Stator-Rotor Differential Protection

The stator and rotor windings in a wound-rotor asynchronous generator are magnetically coupled. The air gap between their magnetic cores and the rotation of one winding against the other make the formulation of the ampere-turn balance equations more complex than in other applications. Nonetheless, this ampere-turn balance allows us to devise a protection element that spans both the stator and rotor and is capable of detecting phase and turn faults in either winding.

The principle of ampere-turn balance is commonly used when protecting power transformers [11]. When the windings that are tied with the ampere-turn balance move against one another, such as in rotating machines, writing the ampere-turn balance equation is not straightforward. In the case of a synchronous generator, we balanced the ampere-turns between the negative-sequence current in the stator and the double-frequency component in the field current (the term double-frequency refers to twice the frequency of the stator voltages and currents) [10]. In this section, we derive the stator-rotor ampere-turn balance differential protection element for a wound-rotor asynchronous generator.

### A. Principle of Operation

In a wound-rotor asynchronous generator, both the stator and rotor windings are three-phase windings. It is convenient to represent the three phase currents by their direct (d), quadrature (q), and zero-sequence (0) components in Park's rotating reference frame. In a stator winding, the d-axis stator current is decoupled from the q-axis stator current. Similarly, in a rotor winding, the d-axis rotor current is decoupled from the q-axis rotor current. In Park's rotating reference frame, the d-axis and q-axis equivalent windings are stationary. We can select the rotating reference frames for the rotor and the stator in such a way that the stationary d-axes in the stator and rotor align (the stationary q-axes in the stator and rotor would also align as a result). In such a case, the stator d-axis current only couples with the rotor d-axis current and the stator q-axis current only couples with the rotor q-axis current. As a result, we can derive a differential protection element that balances the stator and rotor d-axis currents. Additionally, we can derive a second differential protection element that balances the stator and rotor q-axis currents. Of course, the balance must account for the stator and rotor turns ratio.

Reference [12] describes such d-axis and q-axis differential elements applied to a wound-rotor asynchronous generator. The stator and rotor q-axis currents do not match perfectly because of the magnetizing current. Reference [12] proposes using voltages to compensate for the difference.

A significant disadvantage of the method proposed in [12] is that it requires three angular position signals to calculate the d-axis and q-axis current components in the common reference frame (to align the stator d-axis with the rotor d-axis). These angular position signals include:

- The stator rotating field position respective to the stator.
- The rotor rotating field position respective to the rotor.
- The rotor position respective to the stator.

Voltage-based stator and rotor phase lock loops (PLLs) that work with the stator and rotor voltages, respectively, can be used to obtain the first two angular position signals. A rotor position encoder can be used to obtain the rotor position respective to the stator.

However, the rotor position encoder adds a failure mode to the protection scheme and the PLLs may exhibit transient errors as the voltages change and shift during external faults. Also, the rotor voltage that is supplied by an inverter is heavily distorted even during steady-state conditions, and it may change and shift significantly when the crowbar (shorting device) in the rotor circuit closes or opens. PLL errors can cause a spurious differential current in the differential element that balances currents obtained by using the PLLs. Additionally, reliance on voltages from both the stator and rotor would make the differential element less reliable (current-only differential elements are preferred).

### B. Improved Principle of Operation

Our approach eliminates the need for angular position signals. We observe that the d-axis and q-axis current components are orthogonal components of a rotating current vector and focus on the magnitude of that vector:

$$i_S = \sqrt{i_{Sd}^2 + i_{Sq}^2}, \quad i_R = \sqrt{i_{Rd}^2 + i_{Rq}^2} \tag{2}$$

If, as we explained in Subsection IV.A, the d-axis current in the stator matches the d-axis current in the rotor and the q-axis current in the stator matches the q-axis current in the rotor (neglecting the magnetizing current), then the vector magnitudes given by (2) will also match between the stator and rotor.

Because the expressions in (2) only encode magnitudes of the stator and rotor currents, we expect them to be independent of the angular position signals and their individual reference frames. To prove it, we use the general Park transformation equation for the stator phase currents $i_A$, $i_B$, and $i_C$:

$$\begin{bmatrix} i_d \\ i_q \end{bmatrix} = \frac{2}{3} \cdot \begin{bmatrix} \sin(\Theta) & \sin(\Theta - 120°) & \sin(\Theta + 120°) \\ \cos(\Theta) & \cos(\Theta - 120°) & \cos(\Theta + 120°) \end{bmatrix} \cdot \begin{bmatrix} i_A \\ i_B \\ i_C \end{bmatrix} \tag{3}$$

where $\Theta$ is the angle of the rotating reference frame.

We calculate the $i_S$ and $i_R$ current magnitudes per (2) and obtain the following equivalent current:

$$\begin{aligned} i &= \sqrt{i_d^2 + i_q^2} \\ &= \frac{2}{3\sqrt{2}} \sqrt{(i_A - i_B)^2 + (i_B - i_C)^2 + (i_C - i_A)^2} \end{aligned} \tag{4}$$

Equation (4), illustrated with a flow chart in Fig. 4, has the following key properties:

- The equivalent current is independent of the angular position of the reference frame.

- The equivalent current ties together instantaneous values of the phase currents and therefore does not require phasors and by extension does not require frequency measurements. This advantage is especially important given 1) the vast difference between the stator and rotor frequencies and 2) the possibility of the rotor operating at super-synchronous speed when the rotor phase rotation is opposite to the phase rotation when the rotor operates at sub-synchronous speed.
- The equivalent current excludes the zero-sequence component and therefore is independent of the grounding method of the wye-connected winding to which it is applied (the stator may be resistive-grounded, while the rotor is normally ungrounded; see Fig. 1).

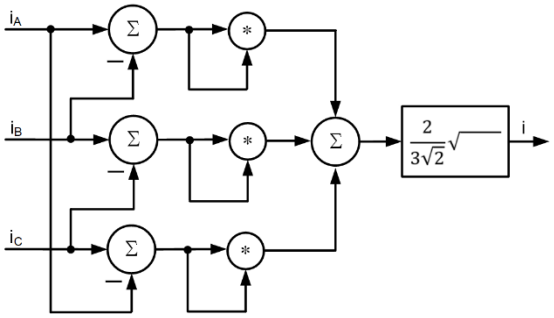


Fig. 4. Flow chart representing the current magnitude calculation (4).

To understand the scaling of the current (4), remember that during balanced three-phase conditions, such as during normal load conditions, (4) gives the value equal to the peak of the phase currents.

Equation (4) allows us to formulate a current-only differential protection element independent of the angular position signals (the stator and rotor voltage-based PLLs and the rotor position encoder).

### *C. Stator-Rotor Differential Protection Element*

Fig. 5 shows a simplified logic diagram of the stator-rotor differential protection (87SR) element for wound-rotor asynchronous generators. The element compares the equivalent currents of the stator ($i_S$) and rotor ($i_R$) obtained by using (4) and adjusted for the turns ratio between the stator and rotor ($N_{RS}$). If we neglect the magnetizing current, these currents match, as long as both the stator and rotor currents are healthy. Differences between the two currents signify an internal fault in either the stator or the rotor (again, neglecting the magnetizing current).

The 87SR element obtains the differential current ($i_{DIF}$) as the absolute value of the difference between the stator and rotor currents. The element is permitted to operate if the differential current is greater than the minimum pickup threshold, 87P.

To address current measurement errors, including saturation of the stator CTs during system faults, the 87SR element obtains the restraining current ($i_{RST}$) as the average of the stator and rotor currents. In this application, both currents are always positive (see (4)), and therefore no magnitude or absolute value operations are required when forming the restraining current. The role of the restraining current is to reflect the stress put on the current-measuring devices and to estimate the measuring errors that may result from that stress in order to use it as a variable threshold for the differential current. Several approaches to restraining can be used, including the maximum value of the two currents or the product of the two currents. Also, a more systematic approach can be taken that evaluates the level of each of the six currents that form the two compared currents as per (4), as discussed in [13].

Additionally, the restraining current can track and hold its past peak value with a decaying time constant on the order of 50 to 100 ms, as follows:

$$i^*_{RST(k)} = MAX\left(i_{RST(k)}, \alpha \cdot i^*_{RST(k-1)}\right) \quad (5)$$

where k is a sample index and $\alpha$ controls the decaying memory ($\alpha < 1$).

Adding the decaying memory of the past peak values (5) improves protection security when the instantaneous restraining current 1) temporarily decreases during an external fault because the instantaneous input currents oscillate and 2) decreases after an external fault is cleared. Equation (5) provides a magnitude-like response, allowing the 87SR element to ride through at the moment when the instantaneous restraining current becomes very small. See the operation examples in Section VI for an illustration of (5).

The 87SR element applies a percentage slope characteristic by multiplying the $i^*_{RST}$ current by the SLOPE factor and obtains the variable threshold (restraint) $i_{RT}$ for the differential current. For simplicity, Fig. 5 omits (5). The 87SR element operates if the differential current is greater than both the minimum threshold (87P) and the restraint ($i_{RT}$).

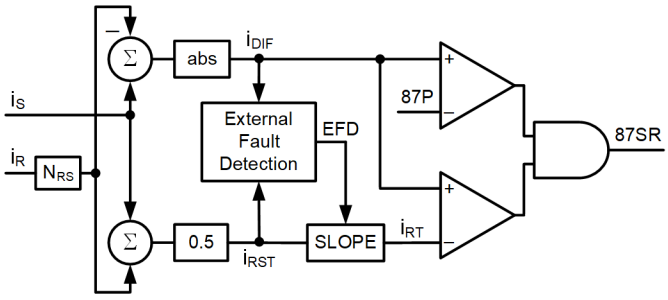


Fig. 5. Simplified 87SR element logic for wound-rotor asynchronous generators.

We recommend that the 87SR element use an external fault-detection (EFD) logic to enhance security and sensitivity. The EFD logic detects external faults and controls the SLOPE multiplier to ensure protection security. If the EFD bit is not asserted, such as during internal faults, the logic keeps the SLOPE small, allowing high sensitivity. If the EFD bit asserts during external faults, the logic raises the SLOPE multiplier to ensure security. Such an EFD-controlled variable-slope method is a better solution than the fixed single- or dual-slope restraining methods because it allows high sensitivity for internal faults while maintaining high security for external faults.

### D. External Fault-Detection Logic

The EFD logic follows a tried-and-true principle that is based on the observation that CTs do not saturate instantaneously but work correctly for at least the initial few milliseconds of a fault even if they subsequently saturate. Therefore:

- During external faults, the differential current remains low while the restraining current rises. The differential current may follow the restraining current if the CTs saturate, but it always lags the restraining current.
- During internal faults, both the differential and restraining currents develop simultaneously.

Fig. 6 shows a simplified diagram of typical EFD logic. For improved performance, the logic responds to the changes (Δ) in the instantaneous differential and restraining currents respective to their one-cycle old values. In general applications to ac currents, the differential and restraining currents are periodic in the steady state before the fault, and therefore the incremental (change) currents are zero before the fault. In the application that uses (4), the differential and restraining currents are constant (dc) in the steady state before the fault, also resulting in the incremental currents of zero.

The EFD logic verifies that the restraining current increased, such as by using a constant threshold $P_R$ of 1.5 pu (1.5 times the stator nominal peak current). The EFD logic verifies that the differential current remains small, such as less than the percentage restraint when using the slope of the restraining characteristic $S_L$ (e.g., 0.20). If the restraining current changes but the differential current does not follow in a set time $T_{EFD}$ (e.g., 3 ms), the EFD logic asserts.

The EFD logic maintains the EFD bit by using the dropout timer $T_{DPO}$ (e.g., 0.5 s). Additionally, the EFD logic can seal-in the output and allow the EFD bit to reset only after the external fault is cleared (i.e., after the restraining current drops below about 150 percent of the stator nominal peak current and the differential current falls below the slope of the restraining characteristic). The EFD logic can also reset the EFD bit to restore full sensitivity and dependability if the external fault is cleared before $T_{DPO}$ expires.

When asserted, the EFD bit enforces high security in the 87SR element, such as by increasing the percentage restraint slope in the 87SR element as shown in Fig. 5.

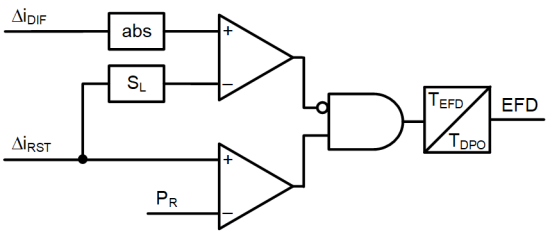


Fig. 6. Typical EFD logic simplified diagram.

The stator differential protection (87S) element can include its own EFD logic. This EFD logic asserts during high-current external faults in the system. The relay can use this EFD logic to secure both the 87S and the 87SR elements.

### E. Current Measurement and Polarity

The 87SR element uses CTs to measure the stator currents, i.e., currents in an ac system with frequency near the system nominal frequency. In contrast, the bandwidth of the rotor currents spans from dc (normal operation) to the nominal system frequency (start up from rotor standstill, considering electrical frequency, irrespective of the number of poles for the stator and rotor). Therefore, the 87SR element must use dc-coupled current-measuring devices for the rotor currents, such as resistive shunts or Hall-effect transducers. During system faults, both the CTs and the rotor current-measuring devices measure transient current components. Therefore, the frequency responses of the two types of sensors (stator CTs and rotor devices) should be matched in the frequency band that the 87SR element uses. Applying low-pass filters to the rotor and stator currents helps with matching the frequency responses of the 87SR element current-measuring devices. These filters can be selected to have a cut-off frequency of several hundred hertz without adversely impacting the 87SR element operating speed.

Because the 87SR element uses measuring devices for the stator and rotor currents that are different in kind, it is beneficial that the percentage restraining operation in Fig. 5 develops separate restraining components for the stator and rotor currents instead of using the average of the two currents to develop a common restraining current. Reference [13] provides details on developing separate restraining components from individual currents instead of developing one common restraining component. Accounting separately for CT errors and rotor current-measuring device errors avoids over-restraining and improves the 87SR element sensitivity without jeopardizing security.

Equation (4) calculates a current magnitude. Therefore, the two compared currents in the 87SR element are always positive. As a result, the 87SR element is insensitive to the current measurement polarity convention in the stator and rotor. Of course, all three phase current measurements must use the same polarity, but the relative polarity convention between the stator and rotor is irrelevant. Also, the rotor currents must be measured on the rotor side of the crowbar so that they always reflect currents in the windings regardless of the position of the crowbar.

### F. Determining the Turns Ratio

You can determine the turns ratio by using the machine nameplate data and verify it by using a recording of a generator operation, calculating the currents (4), and obtaining their ratio. It is good practice to capture records for two or more different conditions in order to verify the turns ratio (such as load and external fault, or two different load conditions). Also, the 87SR element can provide an auto-set feature: it can calculate the turns ratio automatically and use it as a setting after a one-time user command to auto-set the 87SR element turns ratio. The auto-set command is sometimes used in capacitor bank protective relays to effectively remove the standing unbalance in the sensitive capacitor bank protection elements. If used in this application, the auto-set feature would remove the

magnetizing current from the 87SR differential current in the steady-state conditions.

### G. Stator and Rotor Excitation and Saturation

We neglected the magnetic circuit of the machine when deriving the 87SR element. This is no different than when deriving the transformer differential protection element. However, for the proper application of the 87SR element, we need to address the magnetizing current challenge.

The excitation current that flows during normal operation is small, and the 87SR element addresses it by using the minimum pickup threshold.

During external faults, the generator currents rise or exhibit a slowly decaying dc offset. Such a fault response may cause the generator stator or rotor steel to saturate. After the fault is cleared, the increased magnetizing current becomes a larger fraction of the measured currents and may jeopardize the 87SR element security because of insufficient restraining. We address this challenge by using one or more of the following solutions:

- Equation (5) maintains an elevated restraint even after the external fault is cleared. We may use a slower decay with a time constant on the order of 0.5 s to maintain an elevated restraint for a longer time period.
- The EFD logic extends the EFD bit for an extra time period, such as for 1 to 2 s, to force a high SLOPE multiplier and to counter the spurious differential current caused by the saturated core.
- The 87SR element is active for a short time period following the external fault inception, such as for 2 cycles, and is temporarily disabled afterward to avoid the spurious differential current that follows the external fault clearance. An arming logic re-enables the 87SR element in 1 to 2 s following the post-fault steady-state condition.
- The differential and restraining currents are developed as integrals of the classical $i_{DIF}$ and $i_{RST}$ currents in Fig. 5 so that the high restraining current from the time of the fault continues to boost the restraint after the fault is cleared. Of course, the integration should not be perfect, and the integral should "forget" the old values in about 1 to 2 s in order to restore full sensitivity for internal faults. Reference [13] explains this concept in detail.

## V. Differential Element Evaluation Using a Physical Model

To verify the 87SR element principle of operation, we tested the ampere-turn balance concept on a physical wound-rotor asynchronous machine. Because the machine is part of a student lab in a university setting, we were restricted in the types of faults and unbalance conditions we could apply. This restriction was to comply with equipment limitations as well as to prevent any undue stress or damage to the machine or lab facilities.

### A. Model Overview

We performed the laboratory tests on the 220 V, 10 hp (7.5 kW), 4-pole machine shown in Fig. 7. Fig. 8 shows the machine windings. The machine was not equipped yet with rotor- or stator-side converters. Therefore, our options were to use the machine with the rotor short-circuited and operate it as an induction generator or an induction motor.

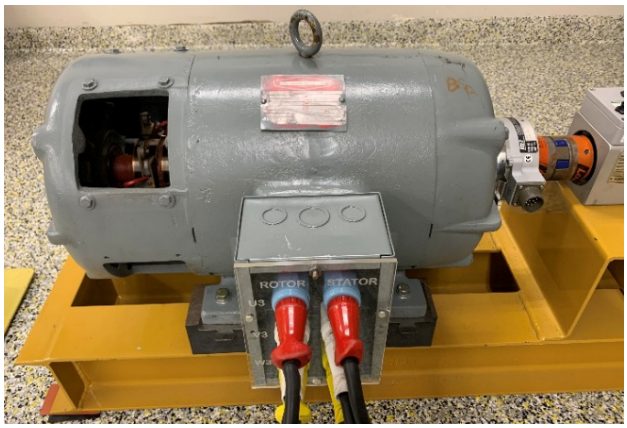


Fig. 7. The 220 V, 10 hp wound-rotor asynchronous machine used for verifying the 87SR element principle of operation.

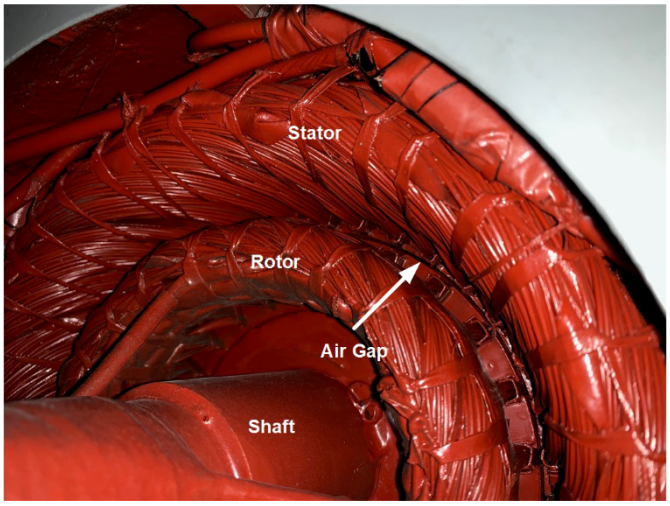


Fig. 8. Windings of the 220 V, 10 hp wound-rotor asynchronous machine.

The machine draws a larger magnetizing current than is typical (the magnetizing reactance is 3 pu) and exhibits a high slip under full load conditions (0.16). We originally tried operating the machine as an induction generator that was feeding an isolated load (auto-excited generator), but the capacitor sizes available for use in the lab either provided too little excitation for the machine or significantly overexcited the machine. When overexcited, the machine drew a magnetizing current that was unreasonably high and prevented an appropriate evaluation of the 87SR element. Given these circumstances, we operated the machine as an induction motor. To avoid placing external faults on the stator side of the machine, we created unbalance conditions in the rotor circuit to verify the ampere-turn balance principle and the 87SR element security that is based on it.

Because the physical machine was not constructed to allow modeling internal turn and winding faults, and we did not want to create high-current faults at the stator terminals, we applied resistive phase-to-phase faults at the stator terminals to upset

the ampere-turn balance and demonstrate the 87SR element dependability.

### *B. Rotor External Resistance Unbalance Test*

While operating the machine as an induction motor, we inserted additional resistance into Phase A of the rotor circuit. Fig. 9 shows the phase and equivalent stator and rotor currents. We do not plot stator voltages because they do not change in any significant way during this event. Similarly, we do not plot the rotor voltages because the rotor windings are short-circuited and the rotor voltages follow the rotor currents and the shorting resistance.

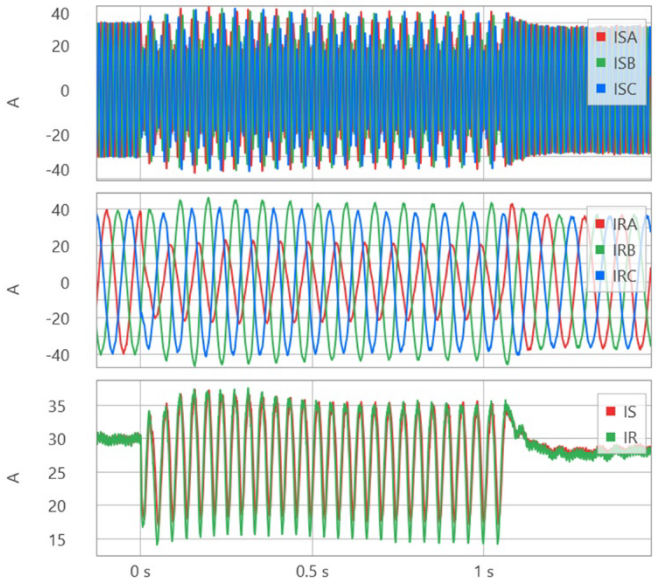


Fig. 9. Currents during a rotor current unbalance condition.

The additional resistor inserted for about 1 s reduces the Phase A rotor current from 40 A peak to about 22 A peak. Because the rotor is ungrounded, the three rotor currents add up to zero at all times. Therefore, when the Phase A current changed, the Phase B and Phase C currents changed slightly too (the rotor zero-sequence current is zero at all times). The rotor current frequency changed from 10.0 Hz before the event to 10.2 Hz after the event. The rotor slowed down from 1,500 rpm to 1,494 rpm, as expected for a motor when the rotor current is temporarily unbalanced and includes the negative-sequence component that produces torque opposing the rotation; we also noticed a change in the sound signature resulting from the current unbalance.

We adjusted the rotor equivalent current (IR) by using a turns ratio of $N_{RS} = 0.77$ to match the stator equivalent current (IS) prior to the resistor insertion (we measured the turns ratio as 0.73, but to provide the best comparison of the transient performance of the 87SR element, we used 0.77 in the examples in this section). The phase currents in the rotor are unbalanced and follow the slip frequency of approximately 10 Hz. The phase currents in the stator are balanced, they follow the system frequency of 60 Hz, but they are modulated at approximately twice the slip frequency, about 20 Hz (see Fig. 10). Despite the differences in frequency, modulation, and symmetry of the stator and rotor phase currents, the stator and rotor equivalent currents matched reasonably well during and after the event (see Fig. 9 and Fig. 10).

The peak difference between the instantaneous values of the equivalent stator and rotor currents is about 17 percent of their peak values. We attribute the mismatch to the magnetizing current (we repeated the test at different stator voltages, and the difference between the equivalent stator and rotor currents follows the stator voltage magnitude).

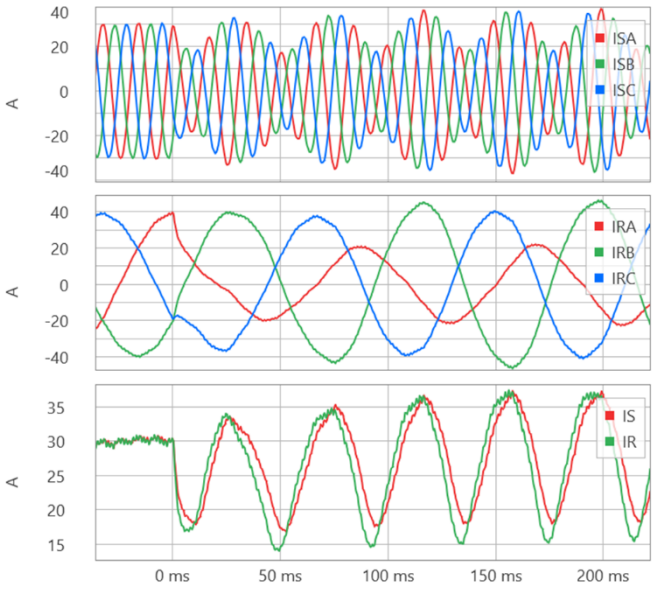


Fig. 10. Zoomed in view of Fig. 9.

### *C. Rotor Open-Phase Test*

While operating the machine as an induction motor, we opened Phase A of the rotor circuit. Fig. 11 shows the phase and equivalent stator and rotor currents. The rotor current frequency changed from 9.8 Hz before the event to 10.1 Hz after the event (the rotor slowed down from 1,506 rpm to 1,497 rpm; we also noticed a change in the sound signature resulting from the current unbalance).

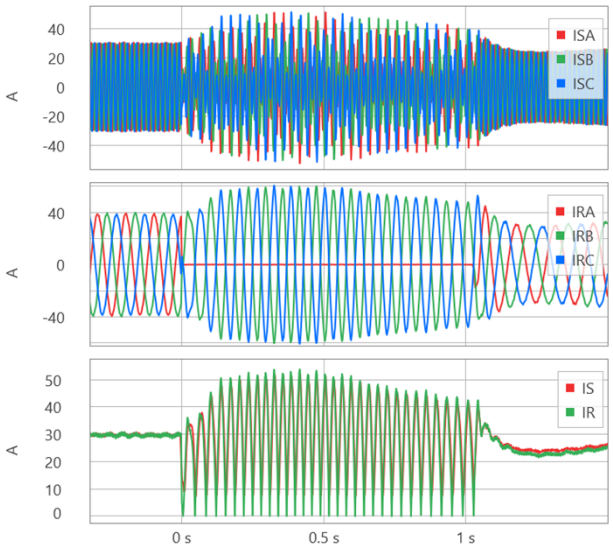


Fig. 11. Currents during a rotor open-phase condition.

Despite the differences in frequency, modulation, and symmetry of the stator and rotor phase currents, the stator and rotor equivalent currents match reasonably well during and after the event (see Fig. 11 and Fig. 12). The peak difference between the instantaneous values of the equivalent stator and rotor currents is about 24 percent of their peak values.

The mismatch is caused by the magnetizing current (we repeated the test at different stator voltages, and the difference between the equivalent stator and rotor currents follows the stator voltage magnitude).

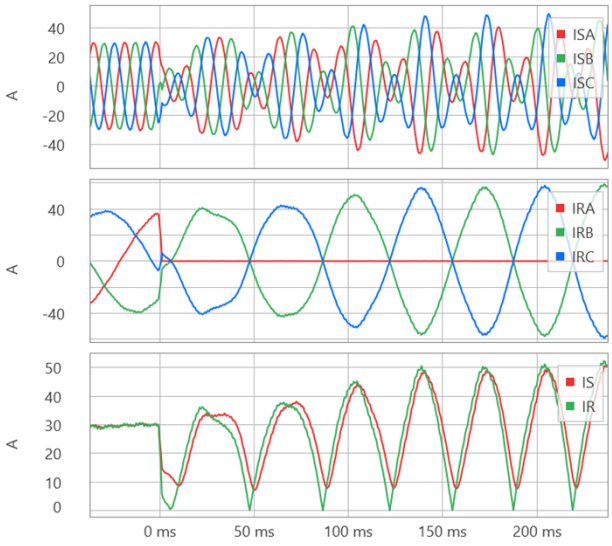


Fig. 12. Zoomed in view of Fig. 11.

This case allows us to approximate the magnetizing current as follows. Because the rotor is ungrounded, the three rotor currents add up to zero at all times. Because $i_{RA} = 0$ during the Phase A open condition, then $i_{RB} = -i_{RC}$. In other words, during this specific unbalance, the Phase B and Phase C rotor currents are identical but have opposite polarities. When these two currents cross zero, all three rotor currents are zero and the equivalent rotor current becomes zero as well. Each time the rotor equivalent current is zero ($i_{RA} = i_{RB} = i_{RC} = 0$, such as at 6 ms, 47 ms, 86 ms, and so on), the stator equivalent current equals the magnetizing current. The stator equivalent current is at the level of 11.4 to 12.2 A when the rotor equivalent current is zero. Therefore, we can state in this case that the peak magnetizing current is at least 11.4 to 12.2 A, or 8.1 to 8.6 A rms (we measured 8.5 A rms during the stator excitation test for the same stator voltage).

### *D. Stator Phase Fault*

While operating the machine as an induction motor, we applied an internal stator phase fault. To avoid damage to the lab equipment and to make the fault detection more challenging, we reduced the fault current by using a 20 Ω resistor in the fault path. Fig. 13 shows the phase and equivalent stator and rotor currents as well as the differential and restraining currents (the restraining current is as per Fig. 5 and uses a 100 percent slope). Before the fault, the rotor speed was 1,524 rpm, resulting in the rotor current frequency of 9.2 Hz.

The stator currents in the faulted phases increase by about 10 A peak or 30 percent during the fault. The rotor currents do not show any appreciable change in magnitude but exhibit a small oscillatory component at about 110 Hz ($2 \cdot 60$ Hz – 9.2 Hz). The stator and rotor equivalent currents differ substantially. The maximum differential current is about 14 A peak, while the restraining current is about 34 A peak. The 87SR element would operate with a slope setting below 40 percent.

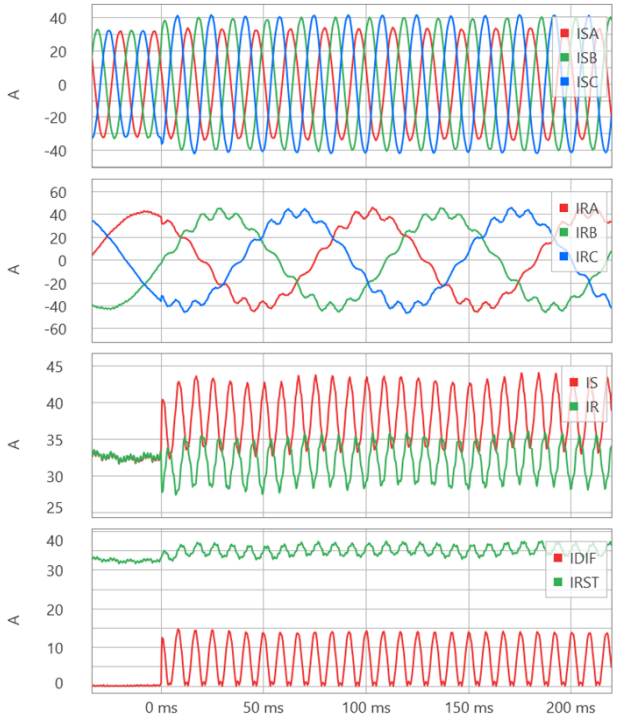


Fig. 13. Currents during a stator BC fault.

## VI. Differential Element Evaluation Using a Digital Simulator

To further verify the 87SR element and to illustrate its operation, we used a digital model of a 333 MW, 18 kV wound-rotor asynchronous machine within the Real Time Digital Simulator (RTDS) package [14] following on the work covered in [15]. The model is capable of simulating internal faults. Our primary focus, however, is on external faults and protection security. The 87SR element sensitivity – as in the case of any protection element – is finite and is a result of the 87SR element design and applied settings. Internal fault simulation results should be treated with caution because the model uses a simple circuit-based method [16] to represent shorted windings and does not account for phenomena such as local iron saturation due to high current in the turn-fault loop or dependance of mutual coupling on the location of faulted turns within the winding. Also, if not cleared promptly, internal faults tend to evolve, making their modeling even more difficult.

Fig. 14 shows the configuration of the modeled system.

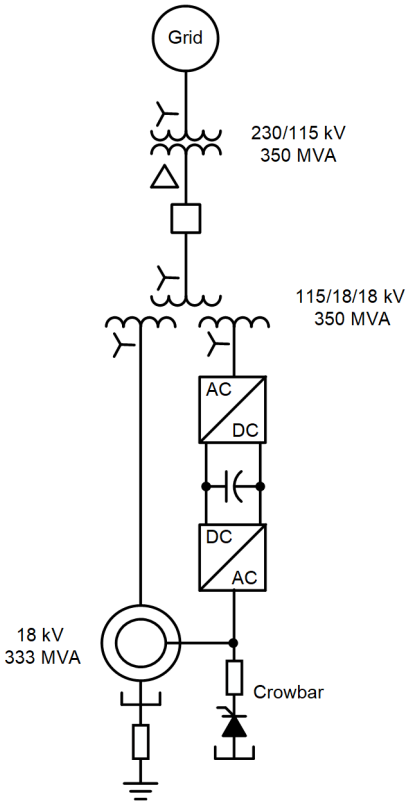


Fig. 14. System configuration and basic data for RTDS simulations.

### A. Model Overview

Both the stator and rotor have two parallel branches per phase. The windings are divided in proportion to the faulted turns to allow internal fault simulations of phase (winding-to-winding), turn, and ground (winding-to-ground) faults. The stator is grounded through high resistance, while the rotor is ungrounded. The machine model includes a nonlinear reactor to represent the magnetizing current.

The model includes a single turbine represented by using a multimass method with a shaft spring, inertia, and damping constants congruent with the machine size and ratings.

The model incorporates multiple control loops, including real power regulation in the generating mode, speed regulation in the pumping mode, reactive power regulation or voltage regulation in both the generating and pumping modes, and finally, the dc bus voltage regulation. The order, time constants, gains, and limiters of the controllers are default values of the RTDS library and are congruent with the machine and turbine size and ratings.

The stator- and rotor-side converters are two-level converters. The model reproduces significant high-frequency ripples in the machine currents that result from the converter switching operation (the RTDS solver works with a 40 μs time step).

The rotor crowbar circuit includes current-limiting resistors. When the crowbar operates, the rotor-side converter ceases to inject the current. We operated the crowbar circuit arbitrarily in order to verify the 87SR element performance with and without the crowbar circuit.

We used the RTDS machine module “RTDS_PD_INDM_FLT” and left all the model parameters at their default values.

Before using the model to simulate external and internal faults, we used it to reproduce the events from the physical model described in Section V. We did not match the machine and system parameters and therefore cannot expect the results to match exactly. However, we were able to reproduce all the key characteristics of the stator and rotor currents. This gives us additional confidence in the validity of both the physical model and the RTDS model.

### B. External High-Current Unbalanced Fault

Fig. 15 plots stator and rotor voltages and currents for a metallic external AB fault at the machine terminals. The ISF and IRF currents are the stator and rotor equivalent currents filtered (label F) with a 2 ms boxcar filter to remove the high-frequency ripple associated with converter switching. The rotor current is referred to the stator side by using the turns ratio of 2.692. IDIF is the differential current and IRST is the restraining current according to (5).

We modeled the following sequence of events:

- 0 ms: fault inception.
- 85 ms: crowbar closes.
- 150 ms: fault clears.
- 180 ms: crowbar opens.

The stator and rotor equivalent currents are constant in the steady state prior to the fault. They match very well during the fault, both when the converter attempts to modulate the rotor currents (0 – 85 ms) and when the rotor currents pass through the crowbar (85 – 150 ms). The stator and rotor currents contain many transients, including high-frequency components and decaying dc components. The resulting equivalent currents are time-varying and follow an irregular pattern. However, on a sample-by-sample basis, the plot shows a nearly perfect match for the stator and rotor currents, as expected based on the ampere-turn balance principle. The differential current remains very small compared with the restraining current, ensuring protection security. The mismatch is slightly higher just after the fault is cleared. We attribute this increased difference to the magnetizing current (the fault currents elevated the flux, especially because they exhibit decaying dc components that offset some currents to the point of not crossing zero, and the flux decays slowly after the fault is cleared).

The differential current does not change much after the restraining current changed at the beginning of the fault, guaranteeing that the EFD logic does assert for this external fault.

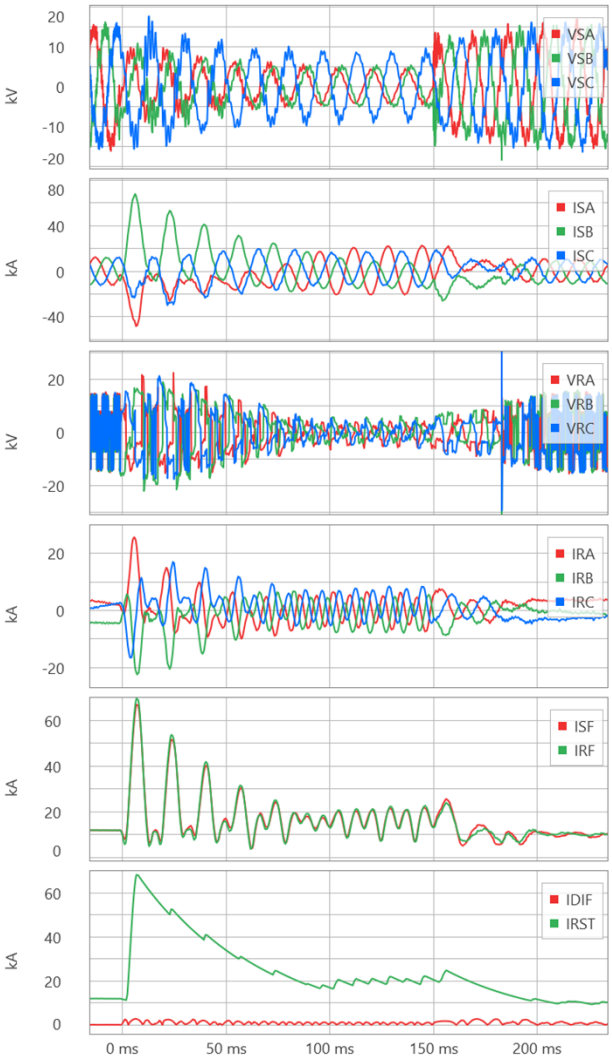


Fig. 15. High-current external AB fault.

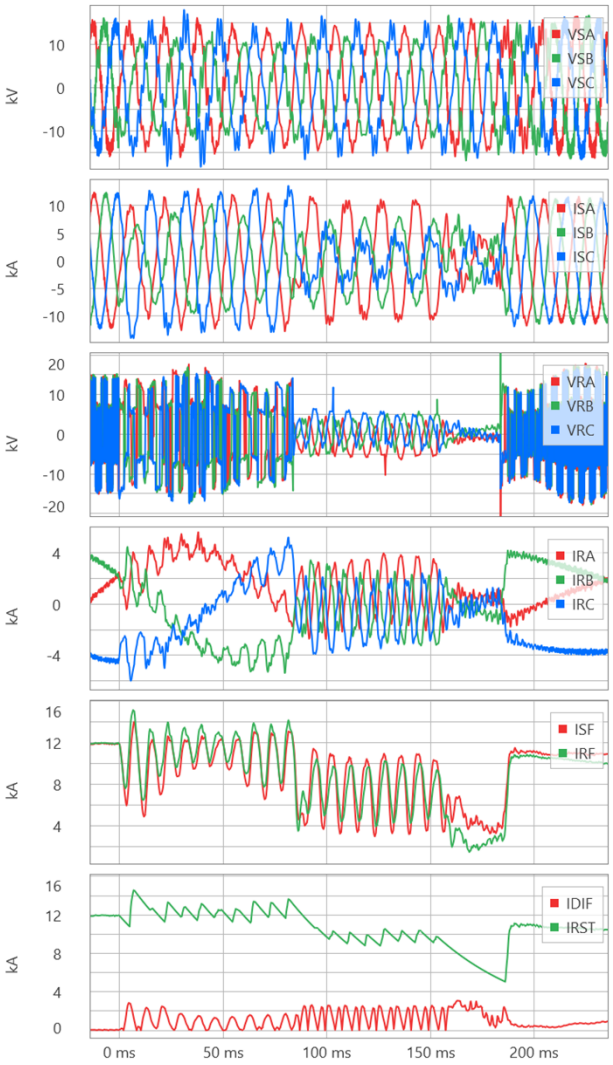


Fig. 16. Low-current external AB fault.

### C. *External Low-Current Unbalanced Fault*

Fig. 16 plots stator and rotor voltages and currents for a low-current external AB fault at the machine terminals. We reduced the fault current on purpose to explore the impact of magnetizing current. The stator and rotor currents remain at the pre-fault level during this fault. The equivalent currents oscillate because the currents are unbalanced. When the crowbar operates, the currents are less than the load current. The stator and rotor equivalent currents match but not perfectly. We attribute the difference to the magnetizing current. Because the fault current is small, the magnetizing current appears larger in proportion to the restraining current. The 87SR element can be restrained with a slope on the order of 30 percent. The mismatch between the equivalent stator and rotor currents becomes slightly higher when the crowbar is closed (after 85 ms).

### D. *Stator Winding Fault*

Fig. 17 plots stator and rotor voltages and currents for a stator internal winding fault with A and B shorted at 10 percent from the stator neutral point. Note that the stator has two windings per phase and the fault involves only one winding. We modeled the crowbar operation and closed it 150 ms into the fault to evaluate the 87SR element operation without and with the crowbar closed.

The fault does not change stator voltages to any significant degree. The rotor controllers maintain the rotor voltage and current until the crowbar closes. After the crowbar closes, the rotor currents are induced from the stator rather than modulated by the converter. The stator currents increase because of the fault but decrease when the crowbar closes. The differences between the equivalent stator and rotor currents are quite pronounced, and the differential current is greater than 30 percent of the restraining current when the crowbar is open and greater than 100 percent after the crowbar closes. The 87SR element operates if it is set with a slope less than 25 percent. In this case, the protection operating conditions are more favorable if the crowbar is closed.

At the beginning of the fault, the differential and restraining currents change simultaneously, guaranteeing that the EFD logic does not assert for this internal fault.

Of course, the 87S element would detect this phase fault, and the 87SR element would provide backup protection.

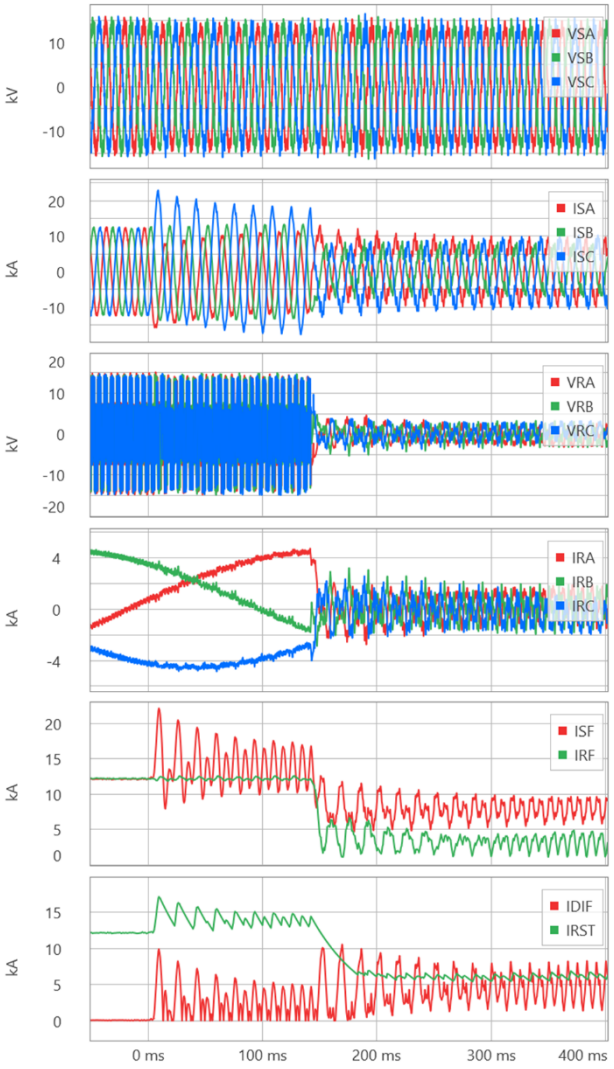


Fig. 17. Stator winding fault.

## E. *Stator Turn Fault*

Fig. 18 plots stator and rotor voltages and currents for a stator turn fault that involves 10 percent of the turns in one of two parallel windings (Phase A). We modeled the crowbar operation and closed it 100 ms into the fault to evaluate the 87SR element operation without and with the crowbar closed.

The fault does not change stator voltages to any significant degree. The rotor controllers maintain the rotor voltage and current until the crowbar closes. After the crowbar closes, the rotor currents are induced from the stator rather than modulated by the converter. The stator currents increase slightly because of the fault but decrease when the crowbar closes. Subsequently, the stator currents show a swing-like response due to rotor speed changes. The differences between the equivalent stator and rotor currents are quite pronounced and the differential current is greater than 30 percent of the restraining current when the crowbar is open, and temporarily greater than 100 percent after the crowbar closes. The swell of stator currents increases the restraining current, but the differential current is still greater than about 20 percent of the restraining current. The 87SR element operates if it is set with a slope less than 25 percent and will remain asserted at all times if the slope is set less than 20 percent. In this case, the protection operating conditions are more favorable during the first few tens of milliseconds after the crowbar closes.

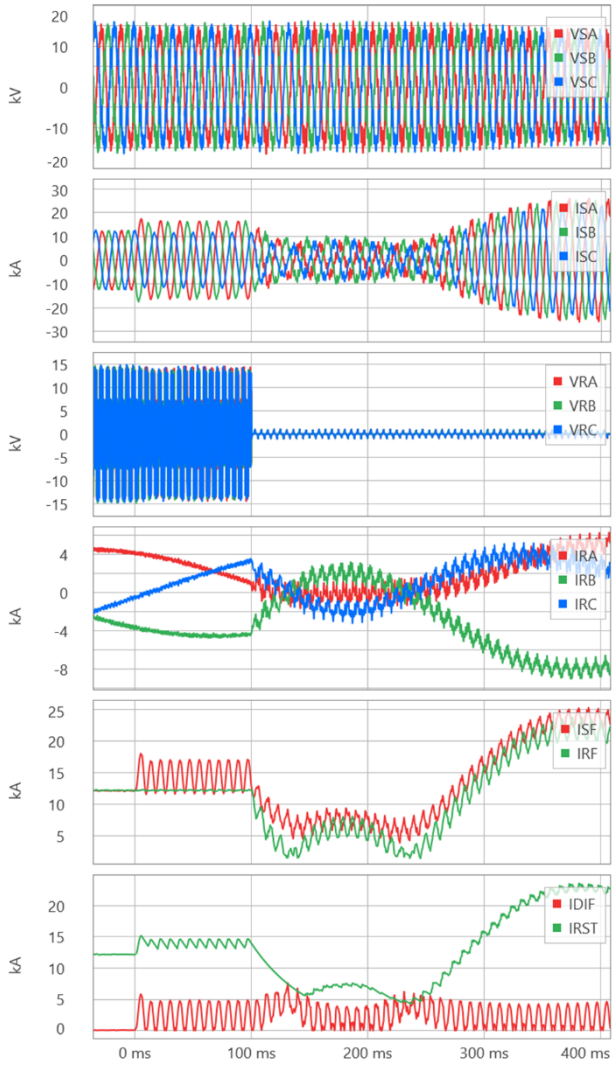


Fig. 18. Stator turn fault.

## F. *Rotor Winding Fault*

Fig. 19 plots stator and rotor voltages and currents for a rotor internal winding fault with A and B shorted at 10 percent from the rotor neutral point. Note that the rotor has two windings per phase and the fault involves only one winding. The fault does not change stator voltages. The rotor controllers maintain the rotor voltage and current. The stator currents change as a result of the fault upsetting the flux. At 50 ms into the fault, the differential current is about 27 percent of the restraining current. The 87SR element operates if it is set with a slope less than 25 percent.

Fig. 20 shows the equivalent stator and rotor currents for a fault lasting 3 s, assuming the crowbar is open and closed (two

different simulations). The plot traces appear thick because of the 120 Hz ripple in the currents (see Fig. 19).

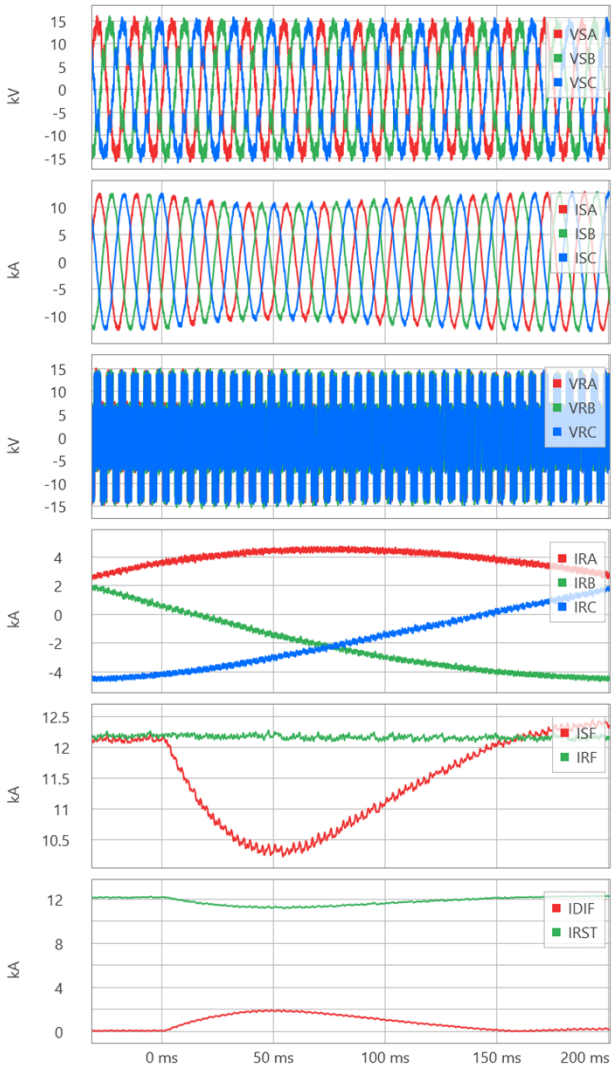


Fig. 19. Rotor winding fault.

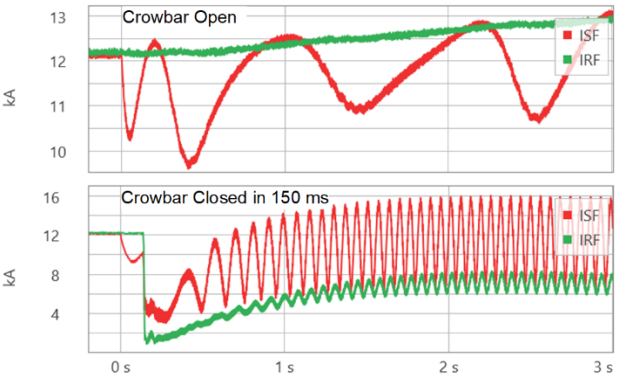


Fig. 20. Stator and rotor equivalent currents for the case of Fig. 19.

When the crowbar remains open, the controllers modulate the rotor current, attempting to keep it constant regardless of the fault. The stator currents change in response to the flux changes caused by the fault. As a result, the difference between the equivalent stator and rotor currents changes over time. This change causes the 87SR element to pick up and drop out approximately every 0.5 s. The controllers are not capable of permanently "erasing" the symptoms of the internal fault, but they may temporarily decrease the 87SR element differential current.

When the crowbar is closed, the system response changes dramatically. The difference between the equivalent stator and rotor currents is more pronounced, resulting in better 87SR element dependability. Both the stator and rotor equivalent currents oscillate, but in this case, the oscillation period is about 60 ms. If the 87SR element were to use an intentional time delay, that delay should not exceed about 20 ms.

### *G. Rotor Turn Fault*

Fig. 21 plots stator and rotor voltages and currents for a rotor turn fault that involves 10 percent of the turns in one of two parallel windings (Phase A). The fault does not change stator voltages. The rotor controllers maintain the rotor voltage and current. The stator currents change slightly as a result of the fault that upsets the flux. At 100 ms into the fault, the differential current is about 10 percent of the restraining current. The 87SR element operates if it is set with a slope less than 10 percent.

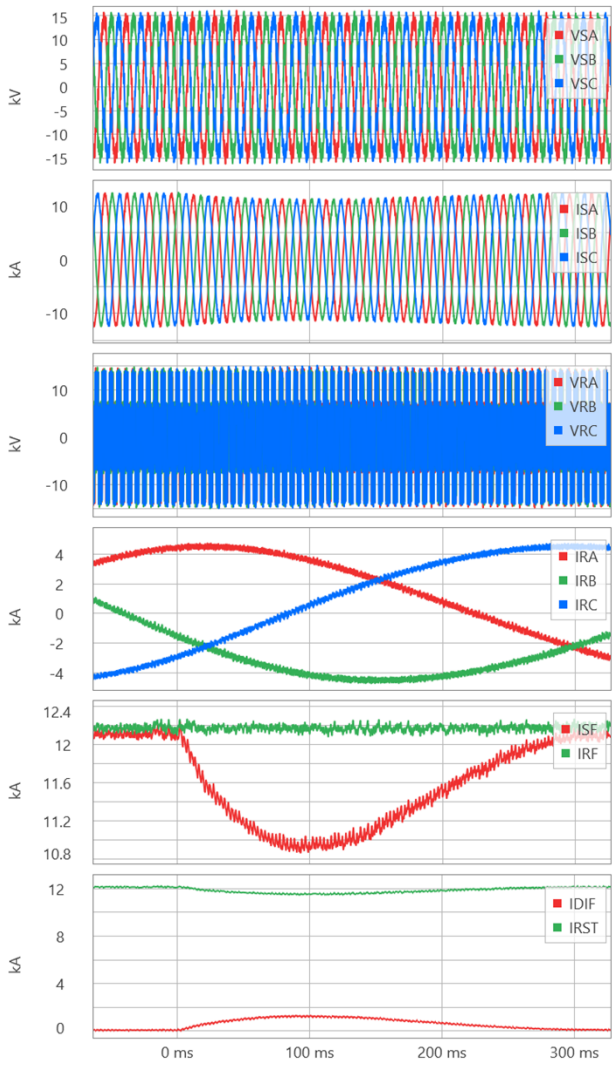


Fig. 21. Rotor turn fault.

Fig. 22 shows the equivalent stator and rotor currents for a fault lasting 3 s, assuming the crowbar is open and closed (two different simulations). The plot traces appear thick because of the 120 Hz ripple in the currents (see Fig. 21).

When the crowbar remains open, the controllers modulate the rotor current, attempting to keep it constant regardless of the fault. The stator currents change in response to the flux changes caused by the fault. As a result, the difference between the equivalent stator and rotor currents changes over time. This change will likely cause the 87SR element to pick up and drop out approximately every 0.5 s. The controllers are not capable of "erasing" the symptoms of the internal fault, but they may temporarily decrease the 87SR element differential current.

When the crowbar is closed, the system response changes dramatically. The difference between the equivalent stator and rotor currents is less pronounced, resulting in a lower 87SR element dependability. However, about 150 ms after the crowbar closed, the differential current increased to as much as 40 percent of the restraining current, giving the 87SR element a chance to operate. Subsequently, the differential current decreased to 5 percent of the restraining current.

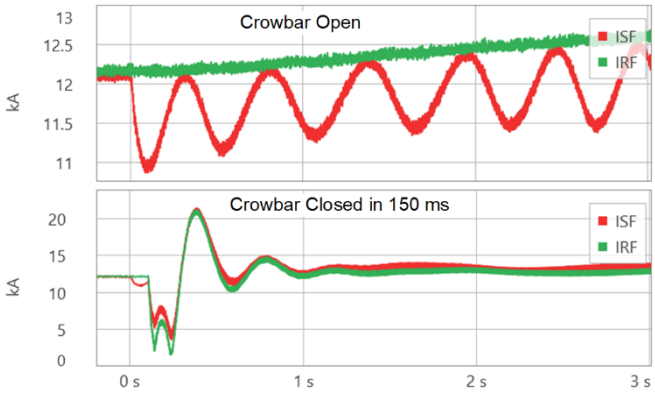


Fig. 22. Stator and rotor equivalent currents for the case of Fig. 21.

## VII. Conclusions

This paper introduced a novel stator-rotor differential protection element for wound-rotor asynchronous generators. The element is based on the ampere-turn balance between the stator and rotor. Therefore, it can detect both phase and turn faults in both the stator and rotor windings. The element balances the magnitudes of Park's (d- and q-axis) current vectors in the stator and rotor and as such avoids the need for aligning the d-q frame references between the stator and rotor. As a result, the element is a current-only element, and it does not require the stator and rotor voltages as references for the rotating electromagnetic fields. The element also does not require the mechanical rotor position encoder to reference the rotor position to the stator.

The paper derives the new protection element and discusses relevant application issues, such as current measurement errors and restraining, security during external faults, current measurement requirements, and magnetizing current.

The paper uses both a scaled-down physical model as well as an RTDS model to illustrate the operation of the new protection element.

The new element is especially beneficial for detecting stator turn faults (the stator differential protection element cannot detect turn faults) and detecting phase and turn faults in the rotor (the rotor differential protection element cannot be applied because rotor currents are not measured at both ends of the rotor winding).

The new protection element is simple and straightforward to implement and set. In applications to smaller machines, such as WTGs, we suggest the machine manufacturer implements the new element as a part of their control package (the WTG controller already has access to both the stator and rotor currents and no new instrumentation or input is required). In applications to large machines, we suggest the new element be included in standalone generator protective relays.

## VIII. Acknowledgements

The authors would like to acknowledge Dr. Herbert Hess and Ms. Salsabil Islam for providing access to and assistance with the University of Idaho physical model of a wound-rotor asynchronous machine and Dr. Ali B. Dehkordi of RTDS, Inc. for his work on developing a digital model of a wound-rotor asynchronous machine and associated controls.

## IX. References

[1] M. M. Mansouri, M. Nayeripour, and M. Negnevitsky, "Internal electrical protection of wind turbine with doubly fed induction generator," Renewable and Sustainable Energy Reviews, Vol. 55, 2016, pp. 840–855, doi.org/10.1016/j.rser.2015.11.023.

[2] IEEE Power & Energy Society Power System Dynamic and Performance Committee, *Advanced Pumped Storage Hydropower Modeling*, Technical Report TR-134, June 2025.

[3] A. Yazdani and R. Iravani, *Voltage-Sourced Converters in Power Systems: Modeling, Control, and Applications*, Wiley, 2010, doi: 10.1002/9780470551578.

[4] E. Nobile, G. Sari, and A. Schwery, "Variable Speed Hydro Pumped Storage as Flexible Enabler of Intermittent Renewable Penetration," 2018 IEEE Power & Energy Society General Meeting (PESGM), Portland, OR, USA, 2018, pp. 1–5, doi: 10.1109/PESGM.2018.8586238.

[5] P. C. Krause, O. Wasynczuk, S. D. Sudhoff, *Analysis of Electric Machinery and Drive Systems*, IEEE Press, 2002.

[6] J. Fraile-Ardanuy, J. R. Wilhelmi, J. J. Fraile-Mora, and J. I. Perez, "Variable-speed hydro generation: operational aspects and control," in IEEE Transactions on Energy Conversion, vol. 21, no. 2, pp. 569–574, June 2006, doi: 10.1109/TEC.2005.858084.

[7] Z. Liu, H. Qi, M. Xu, X. Jiang, and Y. Lv, "Optimization and Transient Analysis of Distributed Asynchronous Condenser," in IEEE Access, vol. 10, pp. 45,811–45,819, 2022, doi: 10.1109/ACCESS.2022.3168971.

[8] A. C. Ferreira, L. M. Souza, and E. H. Watanabe, "Improving power quality with a variable speed synchronous condenser," 2002 International Conference on Power Electronics, Machines and Drives (Conf. Publ. No. 487), IEE, University of Bath, UK, 2002, pp. 456–461, doi: 10.1049/cp:20020160.

[9] H. Huang and X. Chu, "Improving rotational inertia of power system with variable speed synchronous condenser," 2017 IEEE Power & Energy Society General Meeting, Chicago, IL, USA, 2017, pp. 1–5, doi: 10.1109/PESGM.2017.8274191.

[10] B. Kasztenny, N. Fischer, H. J. Altuve, and D. Taylor, "Generator Turn-to-Turn Fault Protection Using a Stator-Rotor-Bound Differential Element," chapter in Synchronous Generator Protection and Control, SEL 2019, ISBN: 978-0972502696.

[11] B. Kasztenny, M. Thompson, and N. Fischer, "Fundamentals of Short-Circuit Protection for Transformers," proceedings of the 63rd Annual

Conference for Protective Relay Engineers, College Station, TX, March 2010.

[12] M. E. Zarei, C. A. Platero, C. V. Nicolás and J. R. Arribas, "Novel Differential Protection Technique for Doubly Fed Induction Machines," in IEEE Transactions on Industry Applications, vol. 55, no. 4, pp. 3,697–3,706, July–Aug. 2019, doi: 10.1109/TIA.2019.2914886.

[13] B. Kasztenny and S. Samineni, "Transformer Differential Protection Revisited," proceedings of the 51st Annual Western Protective Relay Conference, Spokane, WA, October 2024.

[14] Real Time Digital Simulator User's Manual, RTDS Technologies, Inc.

[15] A. B. Dehkordi, D. Finney, R. Chowdhury, and N. Fischer, "Protection validation testing of doubly-fed induction machines using a real-time digital simulator," 19th IET Conference on Developments in Power System Protection (DPSP Europe 2025), Bilbao, Spain, 2025, pp. 255–264, doi: 10.1049/icp.2025.1078.

[16] A. B. Dehkordi, P. Neti, A. Gole, and T. Maguire, "Development and validation of a comprehensive synchronous machine model for a real-time environment," 2009 IEEE Power & Energy Society General Meeting, Calgary, AB, Canada, 2009, pp. 3,330, doi: 10.1109/PES.2009.5275300.

## X. BIOGRAPHIES

**Bogdan Kasztenny** has 35 years of experience in power system protection and control. In his decade-long academic career (1989–1999), Dr. Kasztenny taught power system and digital signal processing courses at several universities and conducted applied research for several relay manufacturers. In 1999, Bogdan left academia for relay manufacturers where he has since designed, applied, and supported protection, control, and fault-locating products with their global installations numbering in the thousands. Bogdan is an IEEE Fellow, an IET Fellow, a Senior Fulbright Fellow, a Distinguished CIGRE Member, and a registered professional engineer in the province of Ontario. Bogdan has served as a Canadian representative of the CIGRE Study Committee B5 (2013–2020) and on the Western Protective Relay Conference Program Committee (2011–2020). In 2019, Bogdan received the IEEE Canada P. D. Ziogas Electric Power Award. Bogdan earned both the Ph.D. (1992) and D.Sc. (Dr. habil., 2019) degrees, has authored over 250 technical papers, and holds over 60 U.S. patents.

**Dale Finney** received his BS degree in engineering from Lakehead University, and his Master of Engineering degree from the University of Toronto, Canada. He began his career with Ontario Hydro, where he worked as a protection and control engineer. Currently, he is employed as a principal power engineer with Schweitzer Engineering Laboratories, Inc. He holds more than a dozen patents and has authored more than 30 papers in the area of power system protection. He is a member of the main committee and past chair of the rotating machinery subcommittee of the IEEE PSRC committee. He is a senior member of the IEEE and a registered professional engineer in the province of Nova Scotia.

**Douglas Taylor** received his BSEE and MSEE degrees from the University of Idaho in 2007 and 2009. He joined Schweitzer Engineering Laboratories, Inc. (SEL) in 2009 and worked as a protection engineer and a research engineer in the Research and Development division. In 2019, Doug joined the system protection group at Avista Utilities and served as a principal protection engineer. Doug rejoined SEL as a senior engineer in 2024. He is a registered professional engineer in the state of Washington, is a member of IEEE, and was formerly a member of the Western Protective Relay Conference (WPRC) planning committee. Doug was selected to participate in the National Academy of Engineering (NAE) 24th Annual U.S. Frontiers of Engineering Symposium. Doug's main interests are power system protection and power system analysis. He holds 4 patents and has coauthored over 20 technical papers in the area of power system protection.